JBIC Journal of Biological Inorganic Chemistry (2023) 28:29–41
https://doi.org/10.1007/s00775-022-01971-2

ORIGINAL PAPER

Exploring the in vitro anticancer activities of Re(I) picolinic acid and its fluorinated complex derivatives on lung cancer cells: a structural study

Mabu L. Matlou[1] · Frederick P. Malan[2] · Sanah Nkadimeng[3] · Lyndy McGaw[4] · Vuyelwa J. Tembu[1] · Amanda-Lee E. Manicum[1]

Received: 24 June 2022 / Accepted: 4 October 2022 / Published online: 4 December 2022

Abstract

Fifteen rhenium(I) tricarbonyl complexes of the form *fac*-[Re(*N,O'*)$(CO)_3$(X)], where *N,O'*-bidentate ligand = 2-picolinic acid (Pico); 3,5-difluoropyridine-2-carboxylic acid (Dfpc); 3-trifluoromethyl-pyridine-2-carboxylic acid (Tfpc) and X = H_2O; pyrazole (Pz); pyridine (Py); imidazole (Im); and methanol (CH_3OH) were synthesized using the '2 + 1' mixed ligand approach with an average yield of 84%. The complexes were characterized using the following spectroscopic techniques: IR, ^{1}H and ^{13}C NMR, UV/Vis, and single-crystal X-ray diffraction. The effect of the fluorine atoms on the backbone of the *N,O'*-bidentate ligand was investigated and a trend was noticed in the carbonyl stretching frequencies: with Pico < Tfpc < Dfpc. The in vitro biological screening on Vero (healthy mammalian), HeLa (cervical carcinoma) and A549 (lung cancer) cells revealed one toxic complex, *fac*-[Re(Pico)$(CO)_3(H_2O)$], with respective LC_{50} values of 9.0 ± 0.9, 15.8 ± 4.9 (SI = 0.570) and 20.9 ± 0.8 (SI = 0.430) µg/mL. As a result, it can be used as a positive control drug of toxicity.

Keywords Rhenium(I) tricarbonyl · Picolinic acid derivatives · Imidazole-based ligands · Crystallography · Cytotoxicity · *N*,*O*-Ligands

Introduction

Humans have been suffering from cancer for a long time, and the oldest documented case was found on ancient Egyptian papyrus documents in 1500 BC [1, 2]. Nevertheless, it was not until the past century that medical science understood cancer and how it develops in the human body [3, 4]. Fortunately, most people diagnosed with this ailment tend to live longer due to the continuous improvement of available treatment such as *cis*-platin and its close derivatives [5, 6]. Furthermore, metal-based drugs have shown to be effective in treating numerous different ailments with applications as antimicrobial agents [7, 8], arthritis treatments [9], anti-ulcer drugs [9], vasodilators [10], diagnostic contrasting agents [11] and anticancer treatments [5]. As already mentioned, *cis*-platin remains the metal-based drug of choice in the treatment of cancer; however, platinum drugs have disadvantages (i.e., side effects), as they continue to face numerous challenges regardless of their widespread use. These side effects are particularly harmful because of their toxic nature, which can cause nephrotoxicity, ototoxicity, and peripheral neuropathy [12]. This has prompted researchers to study other metals like rhenium, particularly the Re(I) tricarbonyl group [13–15]. The cytotoxicity reported by several researchers on Re(I) tricarbonyl complexes and their ability to be used for therapeutic purposes makes this element an essential and attractive drug component [16–19]. Several rhenium complexes were studied and explored for potential anticancer applications for liver cancer, lung cancer, and glioblastoma [20–28]. In addition, the luminescent Re(I) complexes are comprehensively explored for their potential use as imaging agents and as photodynamic therapy (PDT) candidates [29–35]. The *fac*-Re$[(CO)_3(H_2O)_3]^+$ synthon

✉ Amanda-Lee E. Manicum
ManicumAE@tut.ac.za

1 Department of Chemistry, Tshwane University of Technology, P.O. Box X680, Pretoria 0001, South Africa

2 Department of Chemistry, University of Pretoria, 02 Lynnwood Road, Hatfield, Pretoria 0001, South Africa

3 Department of Life and Consumer Sciences, University of South Africa, Private Bag X6, Florida Campus, Florida 1710, South Africa

4 Phytomedicine Programme, Department of Paraclinical Sciences, University of Pretoria, Private Bag X04, Onderstepoort 0110, South Africa

is extensively studied and used because of its coordinated water molecules, which altered chelating ligand systems can proficiently replace with the '2 + 1' mixed ligand model [36–43]. This versatile approach combines a bidentate and a monodentate ligand to synthesize Re(I) tricarbonyl complexes for anticancer applications [14, 26, 35, 44–47].

We employed picolinic acid (Pico) and its fluorinated derivatives in this study (Fig. 1). Pico possesses efficient chelating characteristics and is composed of a six-membered ring with nitrogen and carboxyl groups. This molecule is a metabolic product of the kynurenine pathway, as it generates nicotinamide adenine dinucleotide (NAD^+), which is essential for all living cells [48]. Even though the physiological function of Pico has not been recognized thus far, a variety of biological mediums have been identified as containing this compound (i.e., cell culture supernatants, blood serum cerebrospinal fluid, human milk, pancreatic juice, and intestinal homogenates) [49–51]. According to some reports, involving the cytotoxicity studies of Pico, high concentrations of approximately 1–4 mM of Pico selectively inhibit a diversity of viruses in culture, including Human Immunodeficiency Virus (HIV), Herpes Simplex Virus (HSV), and Simian Virus (SV) in culture [52, 53]. Given the presence of the carboxylic acid molecule in biological systems, it was established that Pico and its fluorinated derivatives, 3,5-difluoropyridine-2-carboxylic acid (Dfpc) and 3-trifluoromethyl pyridine-2-carboxylic acid (Tfpc) should form part of this study as the coordinating bidentate ligand to the Re(I) tricarbonyl synthon, *fac*-$[Re(CO)_3(H_2O)_3]^+$. Therefore, the study aimed to synthesize and characterize a wide range of Re(I) tricarbonyl complexes bearing the picolinic acid bidentate ligand with its fluorinated analogues for the design of a wide range of possible anticancer agents. Herein, the authors describe a series of 15 Re(I) picolinic acid-based complexes of the form *fac*-[Re(*N,O*)$(CO)_3$(X)], where *N,O* = 2-picolinic acid (Pico),

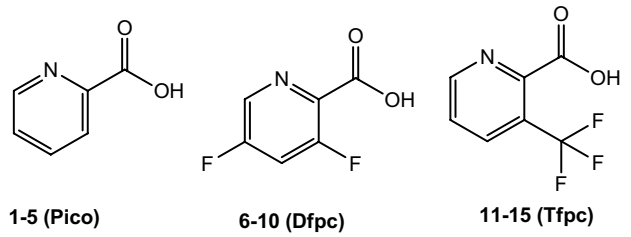

Fig. 1 Picolinic acid derivatives, and their corresponding complex numbers used in this study

3,5-difluoropyridine-2-carboxylic acid (Dfpc) and 3-trifluoromethyl pyridine-2-carboxylic acid (Tfpc); X = H_2O, CH_3OH, Pyridine (Py), Imidazole (Im) and Pyrazole (Pz), which have been synthesized from the precursor aqua complexes: *fac*-[Re(Pico)$(CO)_3(H_2O)$] (**1**), *fac*-[Re(Dfpc)$(CO)_3(H_2O)$] (**6**) and *fac*-[Re(Tfpc)$(CO)_3(H_2O)$] (**11**), in methanol at room temperature as indicated in Scheme 1. We further investigate and comprehensively discuss the solid-state molecular structures of eight complexes: *fac*-[Re(Pico)$(CO)_3$(Pz)] (**2**), *fac*-[Re(Pico)$(CO)_3$(Py)] (**3**), *fac*-[Re(Dfpc)$(CO)_3(H_2O)$] (**6**), *fac*-[Re(Dfpc)$(CO)_3$(Pz)] (**7**), *fac*-[Re(Dfpc)$(CO)_3$(Py)] (**8**), *fac*-[Re(Tfpc)$(CO)_3$(Pz)] (**12**),

Scheme 1 Synthesis of the Re(I) tricarbonyl complexes with different *N,O*'-donor bidentate ligands (2-picolinic acid (Pico), 3,5-difluoropyridine-2-carboxylic acid (Dfpc) and 3-trifluoromethyl pyridine-2-carboxylic acid (Tfpc)) and monodentate ligands (pyrazole (Pz), pyridine (Py), imidazole (Im), aqua (H_2O) and methanol (CH_3OH))

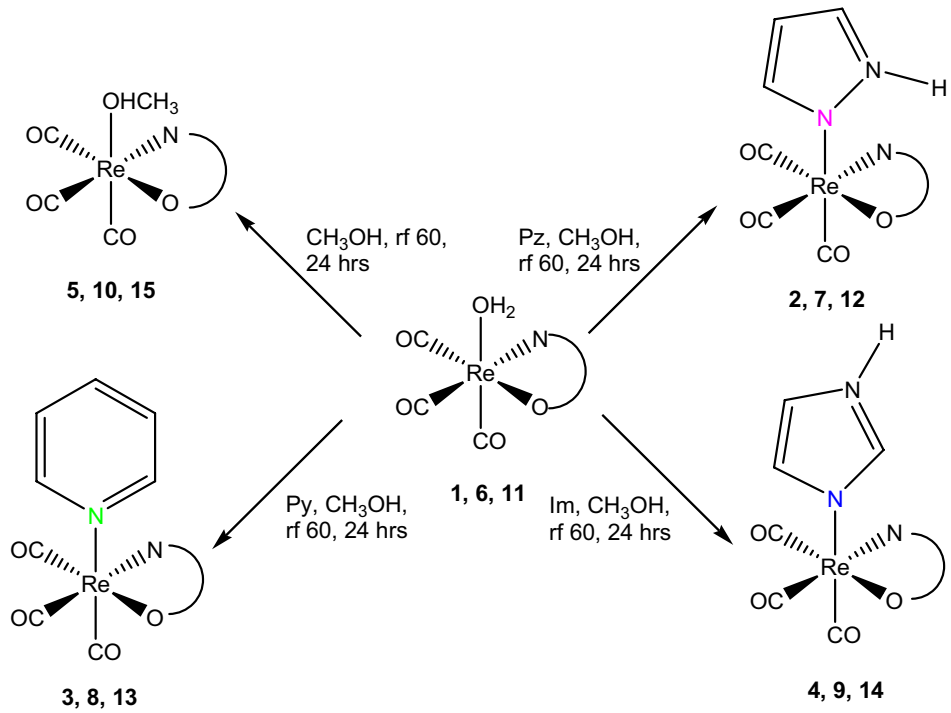

fac-[Re(Tfpc)$(CO)_3$(Py)] (**13**) and *fac*-[Re(Tfpc)$(CO)_3$(Im)] (**14**). Moreover, the cytotoxicity of the 15 synthesized complexes (**1**–**15**) towards Vero cells (healthy mammalian), HeLa (cervical carcinoma) and A549 (lung cancer) cells was examined utilizing the 3-(4,5-dimethyl-2-thiazolyl)-2,5-diphenyltetrazolium bromide (MTT) assay.

Experimental

Materials and methods

Reagents utilized to synthesize and characterize the products formed were purchased from Strem Chemicals Newburyport (USA) and Sigma Aldrich (South Africa) and were of analytical grade, unless stated otherwise. The reagents and organic solvents used for these experiments were not further purified or modified but were used as received. All the experiments were conducted in aerobic conditions using methanol and deionized water at a controlled pH. For infrared (IR) characterization, a PerkinElmer FT-IR Spectrometer Spectrum two, operating in the 4000–370 cm^{-1} region, was used to record the spectra. The IR is connected to a computer and has a built-in temperature cell regulator, accurate to 0.3 °C. All the IR spectra of the synthesized complexes were recorded at room temperature. A PerkinElmer Lambda XLS + Ultraviolet/Visible (UV/Vis) spectrometer was used to collect the UV/Vis data using a 1.000 ± 0.001 cm quartz cuvette cell. The Elemental Analysis was performed at the University of Kwa Zulu Natal. The Nuclear Magnetic Resonance (NMR) data were acquired from a Bruker MHz nuclear magnetic resonance spectrometer operating at 500.00 MHz for ^{1}H and ^{13}C at room temperature with deuterated dimethyl sulfide (DMSO-d_6) as the solvent. Chemical shifts are reported in ppm relative to the DMSO-d_6 (2.50 ppm on ^{1}H NMR and 39.52 ppm on ^{13}C NMR) peak. All coupling constants, *J*, are reported in Hertz (Hz). Scheme 1 illustrates the synthesis of the following complexes: *fac*-[Re(Pico)$(CO)_3(H_2O)$] (**1**), *fac*-[Re(Pico)$(CO)_3$(Pz)] (**2**), *fac*-[Re(Pico)$(CO)_3$(Py)] (**3**), *fac*-[Re(Pico)$(CO)_3$(Im)] (**4**), *fac*-[Re(Pico)$(CO)_3(CH_3OH)$] (**5**), *fac*-[Re(Dfpc)$(CO)_3(H_2O)$] (**6**), *fac*-[Re(Dfpc)$(CO)_3$(Pz)] (**7**), *fac*-[Re(Dfpc)$(CO)_3$(Py)] (**8**), *fac*-[Re(Dfpc)$(CO)_3$(Im)] (**9**), *fac*-[Re(Dfpc)$(CO)_3(CH_3OH)$] (**10**), *fac*-[Re(Tfpc)$(CO)_3(H_2O)$] (**11**), *fac*-[Re(Tfpc)$(CO)_3$(Pz)] (**12**), *fac*-[Re(Tfpc)$(CO)_3$(Py)] (**13**), *fac*-[Re(Tfpc)$(CO)_3$(Im)] (**14**), and *fac*-[Re(Tfpc)$(CO)_3(CH_3OH)$] (**15**).

Synthesis and characterization of complexes

The starting material, *fac*-$[NEt_4]_2[ReBr_3(CO)_3]$, used for the synthesis of the aqua complexes (**1, 6,** and **11**), was prepared using the method presented by Alberto et al. 1996 [54, 55], with some adjustments. These adjustments are: adding the $[Re(CO)_5Br]$ to the reaction mixture (i.e., NEt_4Br in diglyme) as a solid and stirring the reaction mixture at 120 °C for 22 h (as opposed to the reported 115 °C for 4–5 h). Scheme 1 illustrates the synthesis of the complexes (**1**–**18**) investigated in this study. Complexes **1** (previously reported complex) [56], **6** and **11** were synthesized as follows: *fac*-$[NEt_4]_2[ReBr_3(CO)_3]$ (1010 mg; 1.3110 mmol) was dissolved in 15 mL of water (pH 2.2) by stirring for 20 min at room temperature. $AgNO_3$ (668 mg; 3.93 mmol) was added to the solution and stirred for 24 h at room temperature. Pico (165.9 mg; 1.3476 mmol), 3,5-Difluoropyridine-2-carboxylic acid (Dfpc = 217 mg; 1.3640 mmol) and 3-Trifluoromethyl-pyridine-2-carboxylic acid, (Tfpc = 216 mg; 1.2898 mmol) were added, respectively, to the filtrates and stirred for 24 h at room temperature. Light-yellow precipitates formed, the excess solvent was filtered off and the precipitate was left to dry and weighed. Complexes **2**, **7** and **12** were synthesized as follows: **1** (92 mg, 0.2236 mmol), **6** (94 mg, 0.2107 mmol) and **11** (93 mg, 0.1944 mmol) were, respectively, dissolved in 5 mL methanol and mixed with pyrazole (16 mg, 0.2394 mmol) dissolved in 3 mL of methanol. The mixtures were refluxed for 24 h at a temperature of 60 °C and yellow precipitates formed after the evaporation of the excess solvent. The yellow precipitates were recrystallized with cold methanol, forming the desired complexes, which were confirmed with single-crystal X-ray diffraction. Complexes **3**, **8** and **13** were synthesized as follows: **1** (83 mg, 0.2015 mmol), **6** (102 mg, 0.2273 mmol) and **11** (109 mg, 0.2266 mmol) separately dissolved in 7 mL of methanol were reacted with pyridine (16 mg, 0.2015 mmol) and refluxed for 24 h at 60 °C and yellow precipitates formed after the evaporation of the excess solvent. The yellow precipitates were recrystallized with methanol, forming the desired complexes, which were confirmed with single-crystal X-ray diffraction. Complexes **4**, **9** and **14** were synthesized as follows: **1** (93 mg, 0.2258 mmol), **6** (91.8 mg, 0.2052 mmol) and **11** (103 mg, 0.2153 mmol) were individually dissolved in methanol (5 mL) and mixed with imidazole (15 mg, 0.2262 mmol) dissolved in 3 mL of methanol and refluxed for 24 h at a temperature of 60 °C. The solvents were left to evaporate and a yellow precipitate formed which was left to dry and weighed. Complexes **5**, **10** and **15** were synthesized as follows: **1** (89 mg, 0.2019 mmol), **6** (102 mg, 0.2272 mmol) and **11** (100 mg, 0.2098 mmol) were dissolved separately in 10 mL of methanol and refluxed for 24 h at room temperature. The methanol ligand substituted the aqua ligand and the excess solvent was left to evaporate, as reported in previous studies [39, 55]. The yellow precipitates were dried and weighed.

fac-[Re(Pico)$(CO)_3(H_2O)$] (**1**): Yield = 475 mg, 88%; ^{1}H NMR (500 MHz, DMSO-d_6) δ (ppm) 8.81 (d, J = 5 Hz, 1H), 8.29 (t, J = 8 Hz, 1H), 8.10 (d, J = 8 Hz, 1H), 7.82 (t, J = 6 Hz, 1H); ^{13}C NMR (126 MHz, DMSO-d_6): δ (ppm)

198.16, 198.10, 194.88, 172.27, 152.48, 150.14, 141.74, 129.41, 127.10; IR (cm^{-1}): υCO = 2039, 1862; UV/Vis: λ_{max} = 330 nm, ε = 2431 $M^{-1}.cm^{-1}$; Anal. Calc. for $C_9H_6NO_6Re$: C, 26.34; N, 3.41; H, 1.47; Found: C, 26.05; N, 3.32; H, 1.74%.

fac-[Re(Pico)$(CO)_3$(Pz)] (**2**): Yield = 99 mg, 96%; ^{1}H NMR (500 MHz, DMSO-d_6) δ (ppm): 8.96 (d, J = 5 Hz, 1H), 8.22 (t, J = 8 Hz, 1H), 7.97 (d, J = 8 Hz, 1H), 7.90 (s, 1H), 7.83 (t, J = 7 Hz, 1H), 7.42 (s, 1H), 6.32 (s, 1H); ^{13}C NMR (126 MHz, DMSO-d_6): δ (ppm) 197.03, 196.68, 195.80, 172.08, 153.17, 149.77, 141.49, 141.44, 132.93, 129.59, 127.05, 106.94; IR (cm^{-1}): υCO = 2028, 1926, 1866; UV/Vis: λ_{max} = 336 nm, ε = 1835 $M^{-1}.cm^{-1}$; Anal. Calc. for $C_{12}H_8N_3O_5Re$: C, 31.30; N, 9.13; H, 1.75; Found: C, 31.70; N, 8.92; H, 1.76%. The crystals were obtained from a saturated CH_3OH solution at room temperature overnight to yield yellow block-like crystals.

fac-[Re(Pico)$(CO)_3$(Py)] (**3**): Yield = 82 mg, 87%; ^{1}H NMR (500 MHz, DMSO-d_6) δ 9.05 (d, *J* = 5 Hz, 1H), 8.82 (d, *J* = 5 Hz, 1H), 8.56 (s, 1H), 8.24 (t, *J* = 7 Hz, 1H), 8.11 (d, *J* = 8 Hz, 1H), 8.03 (d, *J* = 8 Hz, 1H), 7.96 (d, *J* = 8 Hz, 1H), 7.88 (t, *J* = 6 Hz, 1H), 7.55 (s, 1H); ^{13}C NMR (126 MHz, DMSO-d_6): δ (ppm) 197.45, 197.07, 195.30, 171.91, 153.01, 152.29, 149.44, 141.80, 140.50, 130.06, 127.23, 127.01; IR (cm^{-1}): υCO = 2024, 1911, 1862; UV/Vis: λ_{max} = 340 nm, ε = 1667 $M^{-1}.cm^{-1}$; Anal. Calc. for $C_{14}H_9N_2O_5Re$: C, 35.67; N, 5.94; H, 1.92; Found: C, 36.01; N, 5.73; H, 1.98%. The crystals were obtained from a saturated CH_3OH solution at room temperature overnight to yield yellow block-like crystals.

fac-[Re(Pico)$(CO)_3$(Im)] (**4**): Yield = 95 mg, 91%; ^{1}H NMR (400 MHz, DMSO-d_6) δ 8.92 (dt, *J* = 5, 1.2 Hz, 1H), 8.22 (td, *J* = 8, 1.5 Hz, 1H), 7.99 (m, 1H), 7.81 (ddd, *J* = 8, 5.4, 1.5 Hz, 1H), 7.20 (t, *J* = 1 Hz, 1H), 7.10 (d, *J* = 1 Hz, 1H), 6.82 (t, *J* = 1 Hz, 1H); ^{13}C NMR (126 MHz, DMSO-d_6): δ 198.01, 197.58, 195.89, 172.04, 152.76, 149.84, 141.38, 138.87, 135.55, 129.62, 128.05, 127.13, 118.79; IR (cm^{-1}): υCO = 2020, 1870; UV/Vis: λ_{max} = 325 nm, ε = 1504 $M^{-1}.cm^{-1}$; Anal. Calc. for $C_{12}H_8N_3O_5Re$: C, 31.30; N, 9.13; H, 1.75; Found: C, 31.29; N, 8.70; H, 1.74%.

fac-[Re(Pico)$(CO)_3(CH_3OH)$] (**5**): Yield = 73 mg, 84%; ^{1}H NMR (500 MHz, DMSO-d_6) δ 8.82 (d, *J* = 5 Hz, 1H), 8.30 (td, *J* = 8, 1.5 Hz, 1H), 8.11 (d, *J* = 8 Hz, 1H), 7.83 (dt, *J* = 9, 3 Hz, 1H); ^{13}C NMR (126 MHz, DMSO-d_6): δ (ppm) 198.16, 198.10, 194.87, 172.27, 152.63, 152.48, 150.14, 141.74, 141.56, 129.41, 129.21, 127.10; IR (cm^{-1}): υCO = 2024, 1915, 1881; UV/Vis: λ_{max} = 333 nm, ε = 1 831 $M^{-1}.cm^{-1}$; Anal. Calc. for $C_{10}H_8NO_6Re$: C, 28.30; N, 3.30; H, 1.90; Found: C, 28.00; N, 3.63; H, 1.74%.

fac-[Re(Dfpc)$(CO)_3(H_2O)$] (**6**): Yield = 435 mg, 75%; ^{1}H NMR (500 MHz, DMSO-d_6) δ (ppm) 8.78 (s, 1H), 8.49 (s, 1H); ^{13}C NMR (126 MHz, DMSO-d_6): δ (ppm) 197.70, 197.41, 194.28, 168.49, 163.71, 162.28, 160.14, 159.82, 158.12, 138.90, 135.70, 134.80, 134.58, 119.14, 114.40; IR (cm^{-1}): υCO = 2035, 1869; UV/Vis: λ_{max} = 333 nm, ε = 1893 $M^{-1}.cm^{-1}$; Anal. Calc. for $C_9H_4F_2NO_6Re$: C, 24.22; H, 0.90; Found: C, 24.25; H, 0.92%. The crystals were obtained from a saturated CH_3OH solution at room temperature overnight to yield yellow block-like crystals.

fac-[Re(Dfpc)$(CO)_3$(Pz)] (**7**): Yield = 80.9 mg, 77%; ^{1}H NMR (400 MHz, DMSO-d_6) δ (ppm) 8.94 (s, 1H), 8.40 (s, 1H), 7.94 (s, 1H), 7.61 (d, J = 2 Hz, 1H), 6.37 (t, J = 2 Hz, 1H); ^{13}C NMR (126 MHz, DMSO-d_6): δ (ppm) 196.60, 196.11, 195.24, 168.29, 168.25, 159.76, 159.67, 142.11, 140.00, 139.72, 133.07, 118.94; IR (cm^{-1}): υCO = 2027, 1888; UV/Vis: λ_{max} = 338 nm, ε = 1480 $M^{-1}.cm^{-1}$; Anal. Calc. for $C_{12}H_5F_2N_3O_5Re$: C, 29.09; H, 1.02; Found: C, 29.11; H, 1.00%. The crystals were obtained from a saturated CH_3OH solution at room temperature overnight to yield yellow block-like crystals.

fac-[Re(Dfpc)$(CO)_3$(Py)] (**8**): Yield = 100 mg, 86%; ^{1}H NMR (500 MHz, DMSO-d_6): δ (ppm) 9.03 (s, 1H), 8.60 (d, J = 5 Hz, 2H), 8.40 (t, J = 9 Hz, 1H), 8.04 (t, J = 8 Hz, 1H), 7.57 (t, J = 7 Hz, 2H); ^{13}C NMR (126 MHz, DMSO-d_6): δ (ppm) 197.02, 196.45, 194.71, 168.19, 162.50, 162.03, 160.43, 159.89, 152.53, 140.52, 139.81, 127.04, 119.18; IR (cm^{-1}): υCO = 2024, 1885; UV/Vis: λ_{max} = 330 nm, ε = 1296 $M^{-1}.cm^{-1}$; Anal. Calc. for $C_{14}H_7F_2N_2O_5Re$: C, 33.14; H, 1.39; Found: C, 29.11; H, 1.03%. The crystals were obtained from a saturated CH_3OH solution at room temperature overnight to yield yellow block-like crystals.

fac-[Re(Dfpc)$(CO)_3$(Im)] (**9**): Yield = 81 mg, 80%; ^{1}H NMR (400 MHz, DMSO-d_6) δ 8.91 (m, 1H), 8.40 (ddd, *J* = 11, 9, 2 Hz, 1H), 8.03 (m, 1H), 7.25 (d, *J* = 3 Hz, 1H), 6.96 (d, *J* = 1 Hz, 1H); ^{13}C NMR (126 MHz, DMSO-d_6): δ (ppm) 197.58, 196.91, 195.35, 168.26, 160.24, 139.44, 139.09, 128.48, 119.01, 118.81, 118.65; IR (cm^{-1}): υCO = 2031, 1880; UV/Vis: λ_{max} = 334 nm, ε = 2004 $M^{-1}.cm^{-1}$; Anal. Calc. for $C_{12}H_5F_2N_3O_5Re$: C, 29.09; H, 1.02; Found: C, 29.10; H, 1.03%.

fac-[Re(Dfpc)$(CO)_3(CH_3OH)$] (**10**): Yield = 82 mg, 78%; ^{1}H NMR (400 MHz, DMSO-d_6) δ 8.83 (d, J = 2 Hz, 1H), 8.50 (d, J = 2 Hz, 1H), 3.37 (s, 3H); ^{13}C NMR (126 MHz, DMSO-d_6): δ (ppm) 197.70, 197.41, 194.29, 168.48, 163.76, 138.91, 134.77, 119.14, 114.41; IR (cm^{-1}): υCO = 2031, 1892; UV/Vis: λ_{max} = 329 nm, ε = 2948 $M^{-1}.cm^{-1}$; Anal. Calc. for $C_{10}H_6F_2NO_6Re$: C, 27.79; H, 1.31; Found: C, 27.77; H, 1.33%.

fac-[Re(Tfpc)$(CO)_3(H_2O)$] (**11**): Yield = 493 mg, 84%; ^{1}H NMR (500 MHz, DMSO-d_6): δ (ppm) 9.07 (d, J = 5 Hz, 1H), 8.66 (d6: tri-aqua, J = 8 Hz, 1H), 7.97 (m, 1H); ^{13}C NMR (126 MHz, DMSO-d_6): δ (ppm) 197.96, 197.88, 194.40, 168.84, 156.09, 149.16, 140.33, 129.34; IR (cm^{-1}): υCO = 2031, 1877; UV/Vis: λ_{max} = 333 nm, ε = 2876 $M^{-1}.cm^{-1}$; Anal. Calc. for $C_{13}H_5F_3NO_6Re$: C, 25.11; H, 1.05; Found: C, 25.12; H, 1.03%.

fac-[Re(Tfpc)$(CO)_3$(Pz)] (**12**): Yield = 79 mg, 77%; ^{1}H NMR (400 MHz, DMSO-d_6): δ (ppm) 9.22 (d, J = 7 Hz, 1H), 8.60 (m, 1H), 7.99 (dd, J = 8, 6 Hz, 1H), 7.93 (d, J = 3 Hz, 1H), 7.49 (d, J = 2 Hz, 1H), 6.35 (t, J = 2 Hz, 1H); ^{13}C NMR (126 MHz, DMSO-d_6): δ (ppm) 196.76, 196.53, 195.33, 168.63, 156.87, 148.77, 141.73, 140.20, 133.16, 129.46, 107.03; IR (cm^{-1}): υCO = 2028, 1870; UV/Vis: λ_{max} = 336 nm, ε = 1706 $M^{-1}.cm^{-1}$; Anal. Calc. for $C_{13}H_6F_3N_3O_5Re$: C, 29.61; H, 1.15; Found: C, 29.59; H, 1.14%. The crystals were obtained from a saturated CH_3OH solution at room temperature overnight to yield yellow block-like crystals.

fac-[Re(Tfpc)$(CO)_3$(Py)] (**13**): Yield = 117 mg, 96%; ^{1}H NMR (400 MHz, DMSO-d_6) δ 9.31 (dd, *J* = 6, 1 Hz, 1H), 9.07 (td, *J* = 5, 1 Hz, 1H), 8.67 (dd, *J* = 8, 1 Hz, 1H), 8.59 (m, 1H), 8.04 (tdd, *J* = 8, 3, 2 Hz, 1H), 7.79 (tt, *J* = 8, 2 Hz, 1H), 7.57 (m, 1H), 7.39 (m, 1H); ^{13}C NMR (126 MHz, DMSO-d_6): δ (ppm) 197.13, 196.91, 194.78, 168.51, 156.65, 152.36, 150.11, 148.45, 140.59, 136.63, 129.95, 127.10, 124.40; IR (cm^{-1}): υCO = 2028, 1870; UV/Vis: λ_{max} = 330 nm, ε = 1213 $M^{-1}.cm^{-1}$; Anal. Calc. for $C_{15}H_8F_3N_2O_5Re$: C, 29.61; H, 1.49; Found: C, 29.63; H, 1.49%. The crystals were obtained from a saturated CH_3OH solution at room temperature overnight to yield yellow block-like crystals.

fac-[Re(Tfpc)$(CO)_3$(Im)] (**14**): Yield = 110 mg, 96%; ^{1}H NMR (400 MHz, DMSO-d_6) δ 9.19 (dd, *J* = 5, 1 Hz, 1H), 8.60 (m, 1H), 8.00 (m, 1H), 7.23 (t, *J* = 1 Hz, 1H), 7.04 (d, *J* = 3 Hz, 1H), 6.86 (t, *J* = 1 Hz, 1H); ^{13}C NMR (126 MHz, DMSO-d_6): δ (ppm) 197.70, 197.38, 195.39, 168.63, 156.40, 148.77, 140.06, 139.03, 129.54, 128.07, 118.94; IR (cm^{-1}): υCO = 2024, 1904, 1877; UV/Vis: λ_{max} = 337 nm, ε = 1928 $M^{-1}.cm^{-1}$. Anal. Calc. for $C_{13}H_6F_3N_3O_5Re$: C, 29.61; H, 1.15; Found: C, 29.60; H, 1.16%. The crystals were obtained from a saturated CH_3OH solution at room temperature overnight to yield yellow block-like crystals.

Fac-[Re(Tfpc)$(CO)_3(CH_3OH)$] (**15**): Yield = 76 mg, 74%; ^{1}H NMR (500 MHz, DMSO-d_6) δ 9.08 (d, *J* = 5 Hz, 1H), 8.68 (d, *J* = 8 Hz, 1H), 7.98 (dd, *J* = 8, 6 Hz, 1H); ^{13}C NMR (126 MHz, DMSO-d_6): δ (ppm) 197.96, 197.88, 194.41, 168.85, 156.09, 149.16, 140.39, 129.35; IR (cm^{-1}): υCO = 2026, 1883; UV/Vis: λ_{max} = 347 nm, ε = 1132 $M^{-1}.cm^{-1}$; Anal. Calc. for $C_{11}H_7F_3NO_6Re$: C, 26.83; H, 1.43; Found: C, 26.83; H, 1.42%.

Crystallography

Single crystals of selected complexes **2**, **3**, **6**, **7**, **8**, and **12**–**14** were analyzed on a Rigaku XtaLAB Synergy R diffractometer, with a rotating-anode X-ray source and a HyPix CCD detector. Data reduction and absorption were carried out using the CrysAlisPro (version 1.171.40.23a) software package [57]. All X-ray diffraction measurements were performed at 150(2) K, using an Oxford Cryogenics Cryostat. All structures were solved by direct methods with SHELXTS-2013 [58] and refined using the SHELXL-2013 [58] algorithm. All H atoms were placed in geometrically idealized positions and constrained to ride on their parent atoms. For data collection and refinement parameters, see the SI (Tables S1–S3). The X-ray crystallographic coordinates for all structures have been deposited at the Cambridge Crystallographic Data Centre (CCDC), with deposition numbers CSD 2,150,078–2,150,089. The data can be obtained free of charge from The Cambridge Crystallographic Data Centre via www.ccdc.cam.ac.uk/data_request/cif.

Biological studies

African green monkey kidney (Vero) normal cells, A549 lung cancer, and HeLa cervical carcinoma cells purchased from American Type Culture Collection were used in the study. Cells of sub-confluent cultures were harvested and centrifuged at 200 × g for 5 min and suspended in a growth medium. The growth medium used for the Vero cells was Minimal Essential Medium (MEM, Biocom Africa) supplemented with 0.1% gentamicin (Virbac) and 5% fetal bovine serum (FBS) (Gibco, Sigma Aldrich). The cancer cell lines (A549 and MCF-7) were maintained in Dulbecco's Modified Eagle's medium (DMEM) (Pan Biotech, Separation Scientific) supplemented with 10% FBS and 1% of penicillin (100 units/mL) and streptomycin (100 µg/mL) (Celtic Molecular Diagnostics). The cells were allowed to reach 80% confluence in an incubator (HERAcell 150, Thermo Electron Corp) at 37 °C in a 5% CO_2 atmosphere. Cells were seeded at a concentration of 1×10^4 per well in columns 2 to 12 into a 96-well tissue cultured plate (NEST, Whitehead Scientific). The medium (200 µL) was added to the wells of the first column and used as a blank (no cells), while the last two columns were left untreated and used as controls. The plates were incubated for 24 h at 37 °C in a 5% CO_2 incubator. The medium was then aspirated from the cells and substituted with 200 µL of test compounds at various concentrations (0.025, 0.05, 0.075, 100, 150, and 200 µg/mL) in fresh medium and incubated at 37 °C in 5% CO_2 for 48 h. Doxorubicin (Pfizer Laboratories) was included as a positive control. After 48 h, the medium was removed, and cells were washed with 200 µL of phosphate-buffered saline (PBS). A 100 µL aliquot of fresh medium was added followed by 30 µL of MTT (Inqaba Biotec) solution prepared at a 5 mg/mL concentration in PBS. The cells were incubated for 4 h at 37 °C in 5% CO_2. After incubation, the medium with MTT was carefully removed without disturbing the MTT crystals in the wells. Solubilization solution (50 µL DMSO) was then added, and the plates were gently shaken to dissolve the MTT formazan crystals. The absorbance was read at 570 nm wavelengths and a referenced wavelength of 630 using a microplate reader (Biotek, Synergy HT). The

viability of cells in percentages was calculated using the formula: %Viability = ((Sample Absorbance/control Absorbance) × 100). The results were expressed as the lethal average concentration of a sample necessary to kill 50% of the exposed population of animals or viable cells (LC_{50}), under specific conditions. The tests were done in triplicate and repeated three times at different times.

Results and discussion

Synthesis

The synthesis of 15 complexes (**1**–**15**) is reported in this study, using 3 different *N,O*-donor bidentate ligands (2-Picolinic acid (Pico); 3,5-difluoropyridine-2-carboxylic acid (Dfpc); and 3-trifluoromethyl-pyridine-2-carboxylic acid (Tfpc)) that are coordinated to the *fac*-$[Re(CO)_3]^+$ core to investigate their coordination modes. The Re(I) tricarbonyl complexes were synthesized using the [2 + 1] mixed ligand method [59]. The tri-aqua complex *fac*-$[NEt_4]_2[Re(CO)_3(H_2O)_3]^+$ is synthesized first as the intermediate product, by adding three equivalents of $AgNO_3$ to the starting material *fac*-$[NEt_4]_2[Re(CO)_3Br_3]$. The stirring of the solution for 24 h at pH of 2.2 ensures that the aqua ligands displace all three of the bromide ligands. In the second step, the *N,O*-donor bidentate ligand is added to *fac*-$[NEt_4]_2[Re(CO)_3(H_2O)_3]^+$ to generate the series of *fac*-$[Re(N,O)(CO)_3(H_2O)]$ complexes (**1**, **6**, **11**). The monodentate ligands (Pz, Py, Im, CH_3OH) are then added to the aqua complexes at 60 °C for 24 h to produce complexes **2**–**5**; complexes **7**–**10**; and complexes **12**–**15** in moderate to good yields, 74–96%. Most of the synthesized complexes formed yellow products and all the complexes were fully characterized by spectroscopic methods IR, NMR, and UV/Vis. Complexes **1**–**4** were relatively pure, based on the elemental analysis that was done to determine the purity.

IR characterization

The spectra of the complexes can be found in the Supplementary Information (Figure **S16**–**S29**) and the IR spectral data of the synthesized complexes are listed in Table 1. In complexes **1** and **6** the broad bands at around 3 362 cm^{-1} can be assigned to the stretching frequency of hydroxyl group from the water molecules. The complexes display a C=N peak ranging between 1601 and 1693 cm^{-1}, with a trend noted in complexes **2** (1673 cm^{-1}) and **12** (1693 cm^{-1}), bearing the Pz ligand in the axial position. This could possibly be an effect caused by the electron-withdrawing fluoro atoms on the ligand backbone, causing a higher C=N stretching vibrations. The absorption peaks observed between 772 and 760 cm^{-1} for the complexes are assigned to deformation vibration of the pyridine ring, which confirms that the pyridyl N atom and carboxyl O atom are coordinated with the center metal ion [60]. No definitive trend can be deduced in the complexes, as indicated in complexes **1**, **2** and **3**, with the stretching bands, respectively, noted at 768, 765 and 764 cm^{-1}. All these complexes (**1**–**15**) show the typical carbonyl stretching frequencies with bands in the range of 2035–1862 cm^{-1} [46, 61–63]. A trend is noted in the carbonyl stretching frequencies for the aqua complexes (**1**, **6** and **11**): 2035 cm^{-1} *fac*-[Re(Dfpc)$(CO)_3(H_2O)$] (**6**) > 2031 cm^{-1} *fac*-[Re(Tfpc)$(CO)_3(H_2O)$] (**11**) > 2024 cm^{-1} *fac*-[Re(Pico)$(CO)_3(H_2O)$ (**1**). This trend confirms that 2-Picolinic acid is the *N,O'*-donor bidentate ligand with the better electron donating properties, thus increasing the electron density on the Re(I) metal center as well as the π-backbonding from

Table 1 Summary of the spectroscopic data for complexes **1**–**15**

Complex	υCO (cm^{-1})	λ_{max} (nm)	ε($M^{-1}.cm^{-1}$)
***fac*-[Re(Pico)$(CO)_3(H_2O)$] (1)**	2024, 1862	330	2 431
***fac*-[Re(Pico)$(CO)_3$(Pz)] (2)**	2028, 1926, 1866	336	1 835
***fac*-[Re(Pico)$(CO)_3$(Py)] (3)**	2024, 1911, 1862	340	1 667
***fac*-[Re(Pico)$(CO)_3$(Im)] (4)**	2020, 1870	325	1 504
***fac*-[Re(Pico)$(CO)_3(CH_3OH)$] (5)**	2024, 1915, 1881	333	1 831
***fac*-[Re(Dfpc)$(CO)_3(H_2O)$] (6)**	2035, 1869	333	1 893
***fac*-[Re(Dfpc)$(CO)_3$(Pz)] (7)**	2027, 1888	338	1 480
***fac*-[Re(Dfpc)$(CO)_3$(Py)] (8)**	2024, 1885	330	1 296
***fac*-[Re(Dfpc)$(CO)_3$(Im)] (9)**	2031, 1880	334	2 004
***fac*-[Re(Dfpc)$(CO)_3(CH_3OH)$] (10)**	2031, 1892	329	2 948
***fac*-[Re(Tfpc)$(CO)_3(H_2O)$] (11)**	2031, 1877	333	2 876
***fac*-[Re(Tfpc)$(CO)_3$(Pz)] (12)**	2028, 1870	336	1 706
***fac*-[Re(Tfpc)$(CO)_3$(Py)] (13)**	2028, 1870	330	1 213
***fac*-[Re(Tfpc)$(CO)_3$(Im)] (14)**	2024, 1904, 1877	337	1 928
***fac*-[Re(Tfpc)$(CO)_3(CH_3OH)$] (15)**	2026, 1883	347	1 132

the tricarbonyl ligands. It is also noticed that complexes having the coordinated Dfpc ligand (**5–10**) have the highest carbonyl stretching frequencies, ranging between 2027 and 2035 cm^{-1}, indicating the electron-withdrawing effects of the fluoride atoms on the ligand backbone. The Tfpc complexes (**11–15**) have the second highest carbonyl stretching frequencies, and even though there are three fluoro atoms on this ligand, the carbonyl stretching frequencies are not the highest. This could be because the fluoro atoms are not directly attached to the ring, leading to a less pronounced influence due to inductive effects.

UV/Vis characterization

All 15 of the synthesized complexes in this study show characteristic UV/Vis absorptions of the low-spin d^6 Re(I) metal center. At their low energy region, transitions from a largely metal-based orbital to an orbital that is ligand based is referred to as Metal-to-Ligand charge transfer (MLCT), and are observed with the λ_{max} varying between 330 and 347 nm. No definitive trend could be deduced from the absorption in the ultraviolet region for the complexes **1** to **5**, since no significant influence by the ligands is noted. The calculated molar absorptivities (ε) range between 1132 and 2948 $M^{-1}.cm^{-1}$, respective to complexes **15** and **10**. From the results, it is noted that at wavelengths of 330, 333 and 336 nm, the respective molar absorptivity trends of the complexes are as follows: **1** > **8** > **13** at 330 nm, **11** > **6** > **4** at 333 nm, and **2** > **12** at 336 nm, showing more intense absorption of **1**, **11** and **2** at the indicated wavelengths.

NMR characterization

The ^1H and ^{13}C NMR analyses of the Re(I) tricarbonyl complexes synthesized in this study were conducted in deuterated dimethyl sulfoxide at 25 °C as mentioned in the method. The NMR data acquired show that some of the complexes synthesized are compatible with the proposed structures. In complexes **2**–**4** and **6**–**15**, downfield shifts of the proton adjacent to the nitrogen atom of the *N,O*-bidentate ligands are noted upon coordination ranging from 0.03 to 0.53 ppm compared to the uncoordinated ligands. Complexes with the Dfpc (**6**–**10**) and Tfpc (**11**–**15**) showed the most prominent shifts on the ^1H NMR spectra compared to those with the Pico ligand, this is because these ligands are better π -acceptors. In the ^{13}C NMR of complexes bearing the Pico ligand, coordination of the carboxylate constituent of the ligand is noted by the downfield shifts of its carbonyl upon coordination, from a shift of 168.3 ppm in its free state to an average shift of 172.1 ppm. However, an anomaly is noted for complexes **6**–**10** with the Dfpc ligand, their ^{13}C spectra show no prominent downfield shifts upon coordination. The carbonyl shifts of the Dfpc bearing complexes appeared around 168.4 ppm which is the same chemical shift of the ligand in its uncoordinated state. For complexes **11**–**15**, the ^{13}C spectra show upfield shifts instead of downfield shifts of the carbonyls upon coordination compared to free Tfpc which is abnormal. All 15 complexes showed presence of the tricarbonyls ranging between 194 and 198 ppm.

XRD characterization

As a continuation into the investigation of the effect of the *N*,*O*-ligands and their substituents on the structural and electronic properties of the rhenium complexes, the structural elucidation of selected complexes were performed. Figures 2 and 3 show perspective views of the molecular structures of **2**, **3**, **6**, **7**, **8**, and **12**–**14**. For more information including tables of bond lengths, bond and torsion angles, as well as other crystallographic parameters, see Tables S1–S4 in the Supplementary Information. The structure of **3** corresponds to the published structure of Hayes et al. (CSD refcode PUDVIV), but is included here for structural comparison purposes [64].

In general, all the structures exhibited slightly distorted octahedral geometries around the central rhenium center, with three carbonyl ligands coordinated to Re in a facial manner, along with the *N*,*O*-bidentate ligand in the basal plane, and a monodentate N/O ancillary ligand occupying the remaining apical coordination site. The deviation from the perfect octahedral geometry is mainly due to the *N*,*O* ligand that bends in the direction of the N/O ancillary ligand (Figs. 2 and 3, Table 2), with average bond angles ranging between 79.41(19) and 87.79(18)° (N1–Re1–N2), 78.6(2) and 84.38(9)° (N2–Re1–O1), 92.1(2) and 95.92(13)° (N2–Re1–C_{CO}), and 173.1(2) and 177.1(3)° (N2–Re1–C_{CO}). The bidentate *N*,*O*-ligands also binds strongly to the rhenium center with a relatively small bite angle ranging between 74.61(16)° and 75.90(9) °, compared to analogous N–Re–O angles in related Re(I) complexes [65–68]. Little variation on the Re1–N1 bond length is observed across the range (2.176(4)–2.191(5) Å), whereas the range is more noticeable for the Re1–O1 bond length of between 2.108(5) Å (complex **3**) and 2.146(3) Å (complex **7**). This is reasoned to be due to the increased electron density on the rhenium center (due to the monodentate sigma *N*,*O*-donor ligand, which increases π-back donation to the carbonyl and *N*,*O*-bidentate ligands, essentially strengthening the corresponding Re1–C_{CO} and Re1–O1 bonds and hence shortening of these bonds. For example, comparing complexes **2** and **3** (each with the same Pico ligand present): Complex **3** (featuring a pyridine ligand) shows a shorter Re1–O1 bond as compared to **2** (featuring a pyrazole ligand). The corresponding Re1–C_{CO} (*trans* to *N*,*O* ligand) bonds are also slightly shorter in the case of **3** (1.897(7) Å *vs* 1.910(3) Å (**2**); 1.915(8) Å *vs* 1.925(3) Å (**2**)). The expected elongation of the C_{CO}–O_{CO} bond lengths are

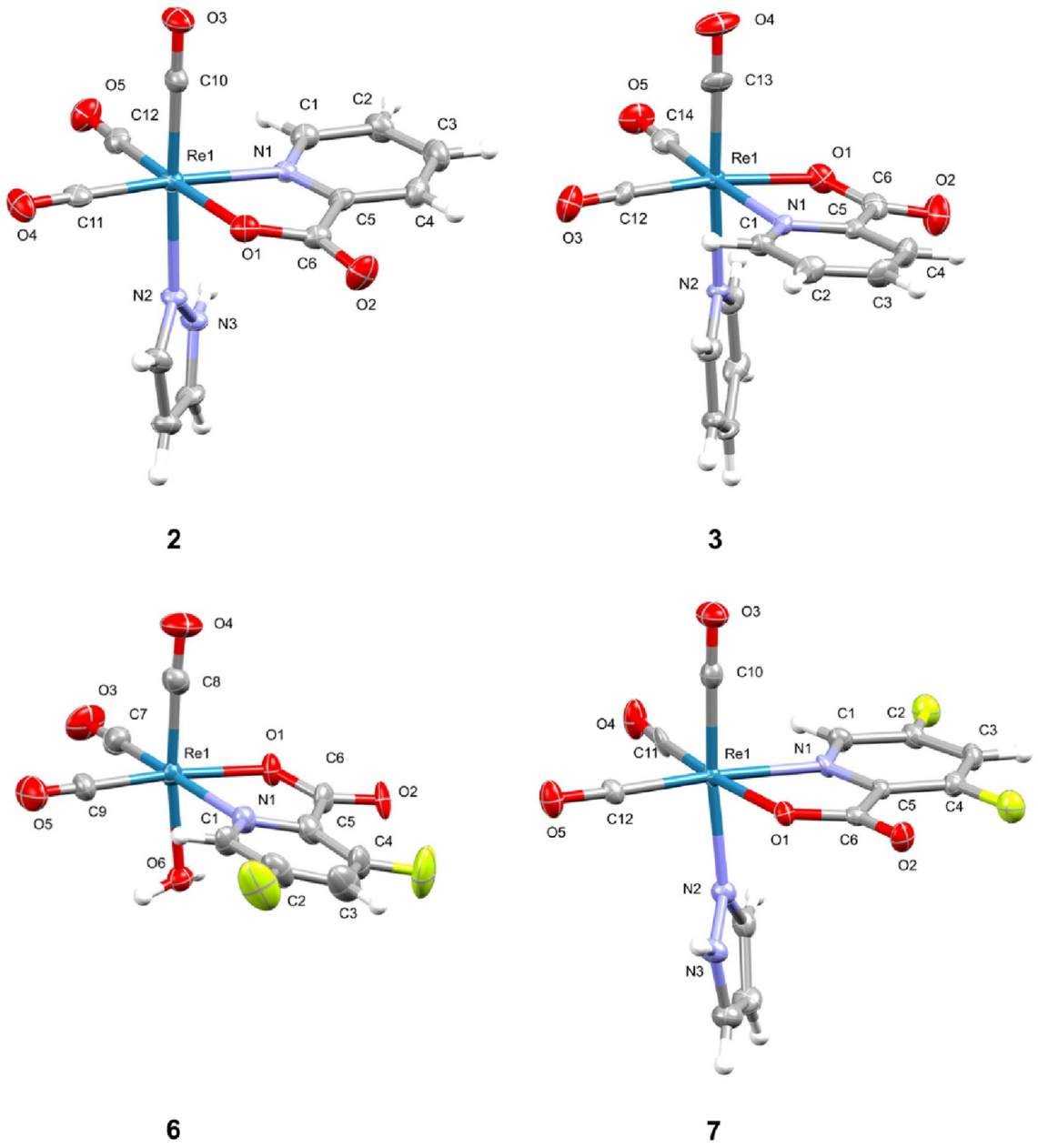

Fig. 2 Molecular structures of complexes **2**, **3**, **6**, and **7** with thermal ellipsoids drawn at 50% probability level

also observed in **3** (1.159(9) Å *vs* 1.149(4) Å (**2**); 1.152(9) Å *vs* 1.145(4) Å (**2**)). Subsequent inclusion of fluorine atoms in the *N*,*O* ligand backbone increases its π-accepting character, with an expected decrease in the Re1–O1 bond lengths (2.145(2) Å (**2**) *vs* 1.1396(19) Å (**12**)). Separated consideration of the electronic effect of monodentate ligands on the resulting complexes leads to similar observations: (i) In the Dfpc ligand series (**6** (H_2O), **7** (Pz), **8** (Py)) the Re1–O1 bond length decreases according to the series Pz > H_2O > Py; (ii) in the Tfpc ligand series (**12** (Pz), **13** (Py), **14** (Im)), the Re1–O1 bond length decreases according to the series Pz > Im > Py. The combination of these two series allows for the ligands to be organized according to decreasing electron donating character according to the series Py > H_2O > Im > Pz. All the other Re–O, Re–C, and Re–N bond lengths appear in the expected range for related complexes [68–71]. Several unique networks of hydrogen bonds were observed in several of the structures studied, particularly between N–H (or O–H) groups (N/O ancillary ligands) and *N*,*O*-ligands (see Figure SI1b in the Supplementary Information). All the complexes, except those featuring Py ligands (**3**, **8**, **13**), exhibited hydrogen bonds. Complexes

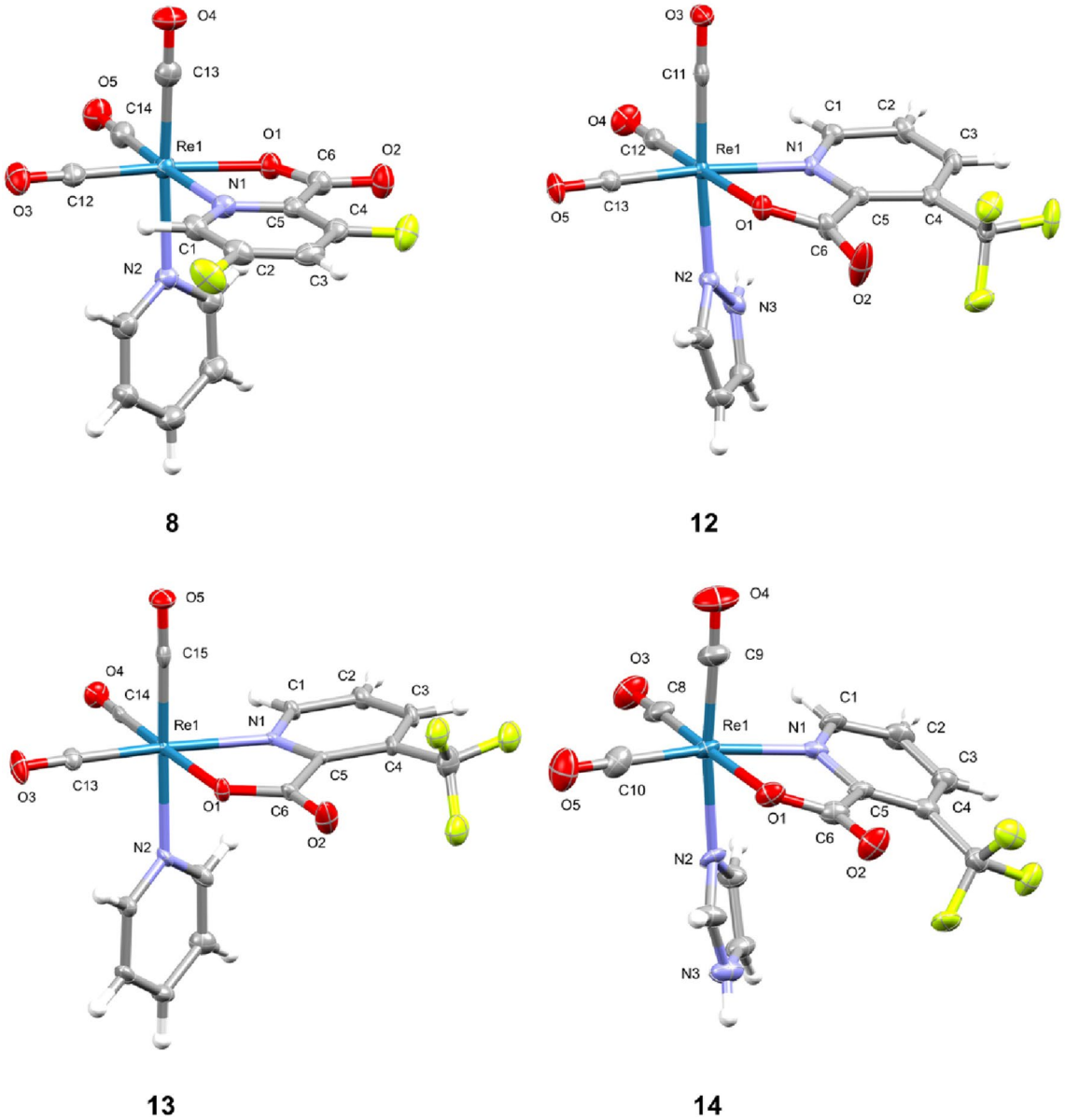

Fig. 3 Molecular structures of complexes **7**, **8**, and **12**–**14**, with thermal ellipsoids drawn at 50% probability level

Table 2 Selected bond lengths and angles of compounds **2**, **3**, **6**, **7**, **8**, and **12**–**14**

Complex	Re1–N1 (Å)	Re1–O1 (Å)	Re1–C_{CO} (*apical*) (Å)	N1–Re1–O1 (°)	X–Re1–N1[a] (°)	X–Re1–O1[a] (°)
***fac*-[Re(Pico)$(CO)_3$(Pz)] (2)**	2.179(3)	2.145(2)	1.923(4)	75.90(9)	85.92(10)	81.46(10)
***fac*-[Re(Pico)$(CO)_3$(Py)] (3)**	2.185(5)	2.108(5)	1.927(7)	75.4(2)	85.1(2)	80.7(2)
***fac*-[Re(Dfpc)$(CO)_3(H_2O)$] (6)**	2.188(7)	2.134(6)	1.924(9)	75.4(2)	80.9(2)	78.6(2)
***fac*-[Re(Dfpc)$(CO)_3$(Pz)] (7)**	2.176(4)	2.146(3)	1.920(5)	74.71(13)	83.38(14)	81.07(13)
***fac*-[Re(Dfpc)$(CO)_3$(Py)] (8)**	2.184(2)	2.124(3)	1.920(3)	75.67(10)	84.05(9)	84.38(9)
***fac*-[Re(Tfpc)$(CO)_3$(Pz)] (12)**	2.184(2)	2.1396(19)	1.913(3)	74.62(8)	83.35(8)	81.36(8)
***fac*-[Re(Tfpc)$(CO)_3$(Py)] (13)**	2.191(5)	2.112(4)	1.915(7)	74.61(16)	87.79(18)	82.73(18)
***fac*-[Re(Tfpc)$(CO)_3$(Im)] (14)**	2.182(6)	2.127(4)	1.917(7)	74.62(18)	79.41(19)	81.56(19)

[a]X = heteroatom (N) in all cases except **6** (O)

7 and **14** each feature two intermolecular N–H···O bonds (2.7971–2.8731 Å between the donor and acceptor atoms; N–H···O angles between 158 and 168°) which links two molecules to form dimers.

The hydrogen-bonding network in complexes **2** and **12** differs in that a one-dimensional chain is formed. The network in each complex structure is formed through a bifurcate hydrogen bond that exists between an N–H bond and two oxygen atoms of the acetate group of an adjacent molecule (2.7763–3.1274 Å between the donor and acceptor atoms; N–H···O angles between 121 and 167°). Structure **6** also forms a one-dimensional chain, although it is unique in that two layers of complex molecules each interact via bifurcate O–H···O bonds: first via the between formation of a chain with an intermolecular O–H···O bond linking adjacent molecules, and secondly via linking two separate chains by the second O–H···O interaction of the bifurcate bond. No mentionable π–π stacking interactions were found in the three-dimensional packing of the structures investigated. The packing along each of the crystallographic axes *a*, *b*, and *c* are unique, apart from complexes **2** and **3**. In the latter case, the two complexes exhibit isostructural features (see Figure SI1a in the Supplementary Information).

Biological studies

Our next objective was to examine the in vitro anticancer activities of the Pico-based complexes (**1**–**15**), in Vero, HeLa and A549 cells with the colorimetric 3-(4,5-dimethylthiazol-2-yl)-2,5-tetrazolium bromide (MTT) assay. The data obtained from this investigation are summarized in Table 3, and Fig. 4 gives a graphical illustration of the LC_{50} values (in µg/mL) obtained from the different cells (Vero and HeLa) versus the positive control (Doxorubicin). LC_{50} represents the concentration that inhibits 50% of growth. The HeLa cells were chosen for this investigation because they are one of the most popular models for assessing chemotherapeutic effects, and they are very well characterized. A549 cells were chosen as their origin is from lung tissue and doxorubicin was the positive control. Table S5 was added with the calculated IC_{50} values of the complexes.

The LC_{50} of complexes **1**–**15** range from 9.0 ± 0.9 to 99.5 ± 4 µg/mL, with the majority of the complexes being

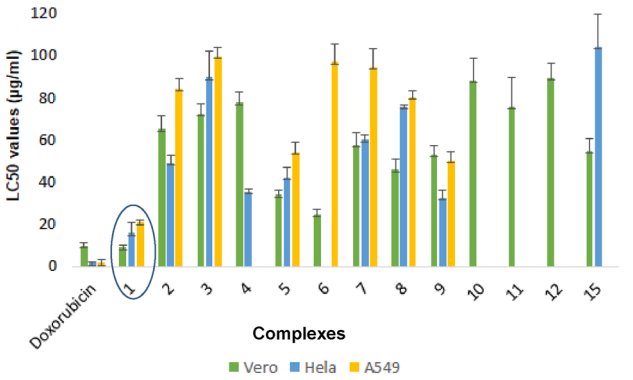

Fig. 4 Graphical representation of the LC_{50} values (concentration inhibiting 50% of growth, values given as (µg/mL)) of each compound (**1**–**15**), against Vero, HeLa and A549 cells, versus the positive control doxorubicin. Data are represented with error bars showing their corresponding standard deviations from three independent experiments with nine replicates

Table 3 A summary of the LC_{50} results obtained from the in vitro cancer screening of complexes **1**–**15** against HeLa, A549 and Vero cells

Complex	Vero LC_{50} (µg/mL)	HeLa LC_{50} (µg/mL)	SI (HeLa)	A549 LC_{50} (µg/mL)	SI (A549)
(1)	**9.0 ± 0.9**	**15.8 ± 4.9**	0.570	**20.9 ± 0.8**	0.430
(2)	65.1 ± 6.3	48.9 ± 3.8	1.105[#]	84.3 ± 4.6	0.772
(3)	72.4 ± 4.4	89.6 ± 12.6	0.808	99.5 ± 4	0.728
(4)	77.7 ± 4.8	35.3 ± 1.3	2.201[#]	> 100	na
(5)	34 ± 2	42.1 ± 4.6	0.808	54.1 ± 5	0.628
(6)	24.5 ± 2.6[a]	> 100	na	97 ± 8.7	0.253
(7)	57.3 ± 5.9	60 ± 2.5	0.955	94.6 ± 8.6	0.606
(8)	45.9 ± 5.1	75.8 ± 0.8	0.606	80.2 ± 2.9	0.572
(9)	53.1 ± 4.1	32.7 ± 3.4	1.624[#]	50 ± 4.2	1.062[#]
(10)	88 ± 10.6[a]	> 100	na	> 100	na
(11)	75.7 ± 14[a]	> 100	na	> 100	na
(12)	89.5 ± 6.8[a]	> 100	na	> 100	na
(13)	> 100	> 100	na	> 100	na
(14)	> 100	> 100	na	> 100	na
(15)	54.5 ± 6[a]	> 100	na	> 100	na
Doxorubicin	9.9 ± 1	1.5 ± 0.5	6.6	1.6 ± 0.4	6.188

[a]More toxic to Vero than to cancerous cell lines; na = not able to be calculated at concentrations tested; [#]promising Selectivity Index (SI) values; most toxic are highlighted in bold

non-toxic towards healthy and cancerous cells. Complex **1** with the Pico bidentate ligand exhibited the highest cytotoxic effect towards HeLa ($LC_{50} = 15.8 \pm 4.9$ µg/mL) and A549 cells ($LC_{50} = 20.9 \pm 0.8$ µg/mL), with comparable toxicity (to the positive control Doxorubicin); however, it was also toxic on the Vero cells ($LC_{50} = 9 \pm 0.9$ µg/mL). Complexes **2** and **4** displayed promising selectivity index (SI) values (of 1.105 and 2.201 respectively) on HeLa cells. Complexes **6**–**10** with the coordinated Dfpc bidentate ligand showed little to no cytotoxicity towards the cancerous lines, with complex **6** being more toxic to healthy Vero cells than cancerous cell lines. Complex **9** had good selectivity on both HeLa and A549 (of 1.624 and 1.062, respectively). The Tfpc-coordinated complexes (**11**–**15**) were found to be the least toxic towards cancerous cells with the majority of the LC_{50} values being > 100 µg/mL against HeLa and A549 cells. Again, complexes **11** and **12** were found to be more toxic to Vero cells as compared to the cancerous HeLa and A549 cells, with respective LC_{50} values of 75.7 ± 14 and 89.5 ± 6.8 µg/mL. Looking at the *N,O*-bidentate ligands used in this study, it is noted that the fluorine atoms present on the ligand backbones of Dfpc and Tfpc have a negative effect on the cytotoxicity of the complexes towards cancerous cell lines.

Conclusion

In this study, the synthesis, spectroscopic characterization (IR, ^{1}H ^{13}C NMR, and UV/Vis) with the solid-state crystal structures of seven complexes, and the in vitro biological applications of the complexes are reported. The IR carbonyl stretching frequencies observed illustrate the electron-withdrawing effect of the fluoro-containing groups of selected *N*,*O*-bidentate ligands. This was furthermore corroborated with the ^{13}C signals of the CO ligands (^{13}C NMR), as well as Re–O, Re–N and Re–C bond lengths (SCXRD). The range of complexes was also evaluated as anticancer agents where the majority of the complexes exhibited low to no toxicity to both healthy and cancerous cells. *fac*-[Re(Pico)$(CO)_3(H_2O)$] showed the highest cytotoxicity towards Vero ($LC_{50} = 9 \pm 0.9$ µg/mL), HeLa ($LC_{50} = 15.8 \pm 4.9$ µg/mL) and A549 cells ($LC_{50} = 20.9 \pm 0.8$ µg/mL). Of the 15 complexes that were used in the in vitro biological study, **1** displayed favorable cytotoxicity (LC_{50}) towards HeLa and A549 cells.

Supplementary Information The online version contains supplementary material available at https://doi.org/10.1007/s00775-022-01971-2.

Acknowledgements We would like to thank the National Research Foundation South Africa (Grant No. 129468), Tshwane University of Technology and the University of Pretoria for institutional and financial support.

Data availability statement The in vitro biological datasets generated during and/or analysed during this study are available from the corresponding author on reasonable request.

Declarations

Conflict of interest There is no conflict of interest to report.

References

1. DeVita VT Jr, Rosenberg SA (2012) Two hundred years of cancer research. New Eng J Med 366:2207–2214
2. Di Lonardo A, Nasi S, Pulciani S (2015) Cancer: we should not forget the past. J Can 6:29–39
3. Hajdu SI (2011) A note from history: landmarks in history of cancer, part 1. Cancer 117:1097–1102
4. Mitrus I, Bryndza E, Sochanik A, Szala S (2012) Evolving models of tumor origin and progression. Tumour Biol J. Int. Soc. Onco. Biol. & Med. 33:911–917
5. Dasari S, Tchounwou PB (2014) Cisplatin in cancer therapy: molecular mechanisms of action. Eur J Pharm 740:364–378
6. Mcquitty RJ (2014) Metal-based drugs. Sci Prog 97:1–19
7. Ip M, Lui SL, Poon VKM, Lung I, Burd A (2006) Antimicrobial activities of silver dressings: an in vitro comparison. J Med Micro 55:59–63
8. Thomas S, McCubbin P (2003) A comparison of the antimicrobial effects of four silver-containing dressings on three organisms. J Wound Care 12:101–107
9. Guo Z, Sadler PJ (1999) Metals in medicine. Ang. Chem. (Int. ed. in Eng) 38:1512–1531
10. Arnold WP, Longnecker DE, Epstein RM (1984) Photodegradation of sodium nitroprusside: biologic activity and cyanide release. Anesthesiology 61:254–260
11. Yan G-P, Robinson L, Hogg P (2007) Magnetic resonance imaging contrast agents: Overview and perspectives. Radiography 13:e5–e19
12. Hartmann JT, Lipp HP (2003) Toxicity of platinum compounds. Exp Op Pharma 4:889–901
13. King AP, Marker SC, Swanda RV, Woods JJ, Qian S-B, Wilson JJ (2019) A rhenium isonitrile complex induces unfolded protein response-mediated apoptosis in cancer cells. Chem. A Eur. J. 25:9206–9210
14. Marker SC, King AP, Granja S, Vaughn B, Woods JJ, Boros E, Wilson JJ (2020) Exploring the in vivo and in vitro anticancer activity of rhenium isonitrile complexes. Inorg Chem 59:10285–10303
15. Delasoie J, Pavic A, Voutier N, Vojnovic S, Crochet A, Nikodinovic-Runic J, Zobi F (2020) Identification of novel potent and non-toxic anticancer, anti-angiogenic and antimetastatic rhenium complexes against colorectal carcinoma. Eur J Med Chem 204:112583
16. Liew HS, Mai CW, Zulkefeli M, Madheswaran T, Kiew LV, Delsuc N, Low ML (2020) Recent Emergence of Rhenium(I) Tricarbonyl Complexes as Photosensitisers for Cancer Therapy. Molecules 25:4179–4199
17. Mkhatshwa M, Moremi JM, Makgopa K, Manicum AE (2021) Nanoparticles functionalised with Re(I) tricarbonyl complexes for cancer theranostics. Int J Mol Sci 22:6546–6563
18. Capper MS, Enriquez Garcia A, Macia N, Lai B, Lin JB, Nomura M, Alihosseinzadeh A, Ponnurangam S, Heyne B, Shemanko CS, Jalilehvand F (2020) Cytotoxicity, cellular localization and photophysical properties of Re(I) tricarbonyl complexes bound to cysteine and its derivatives. J Biol Inorg Chem 25:759–776

19. Ranasinghe K, Handunnetti S, Perera IC, Perera T (2016) Synthesis and characterization of novel rhenium(I) complexes towards potential biological imaging applications. Chem Cent J 10:71–81
20. Darshani T, Fronczek FR, Priyadarshani VV, Samarakoon SR, Perera IC, Perera T (2020) Synthesis and characterization of novel naphthalene-derivatized tridentate ligands and their net neutral rhenium tricarbonyl complexes and cytotoxic effects on non-small cell lung cancer cells of interest. Polyhedron 187:114652–114667
21. Knopf KM, Murphy BL, MacMillan SN, Baskin JM, Barr MP, Boros E, Wilson JJ (2017) In vitro anticancer activity and in vivo biodistribution of rhenium(I) tricarbonyl aqua complexes. J Am Chem Soc 139:14302–14314
22. Murphy BL, Marker SC, Lambert VJ, Woods JJ, MacMillan SN, Wilson JJ (2020) Synthesis, characterization, and biological properties of rhenium(I) tricarbonyl complexes bearing nitrogen-donor ligands. J Org Chem 907:121064–121084
23. Stout MJ, Skelton BW, Sobolev AN, Raiteri P, Massi M, Simpson PV (2020) Synthesis and photochemical properties of Re(I) tricarbonyl complexes bound to thione and thiazol-2-ylidene ligands. Organometallics 39:3202–3211
24. Paparidis G, Akrivou M, Tsachouridou V, Shegani A, Vizirianakis IS, Pirmettis I, Papadopoulos MS, Papagiannopoulou D (2018) Synthesis and evaluation of 99mTc/Re-tricarbonyl complexes of the triphenylphosphonium cation for mitochondrial targeting. Nucl Med Biol 57:34–41
25. Sovari SN, Golding TM, Mbaba M, Mohunlal R, Egan TJ, Smith GS, Zobi F (2022) Rhenium(I) derivatives of aminoquinoline and imidazolopiperidine-based ligands: synthesis, in vitro and in silico biological evaluation against Plasmodium falciparum. J Inorg Bio 234:111905–111915
26. Collery P, Mohsen A, Kermagoret A, Corre S, Bastian G, Tomas A, Wei M, Santoni F, Guerra N, Desmaële D, d'Angelo J (2015) Antitumor activity of a rhenium (I)-diselenoether complex in experimental models of human breast cancer. Invest New Drugs 33:848–860
27. Veena V, Harikrishnan A, Lakshmi B, Khanna S, Desmaele D, Collery P (2020) A New model applied for evaluating a rhenium-diselenium drug: breast cancer cells stimulated by cytokines induced from polynuclear cells by LPS. Anticancer Res 40:1915–1920
28. Domenichini A, Casari I, Simpson PV, Desai NM, Chen L, Dustin C, Edmands JS, van der Vliet A, Mohammadi M, Massi M, Falasca M (2020) Rhenium N-heterocyclic carbene complexes block growth of aggressive cancers by inhibiting FGFR- and SRC-mediated signalling. J. Exp. Clin. Cancer Res. CR 39:276–293
29. Artem'ev AV, Petyuk MY, Berezin AS, Gushchin AL, Sokolov MN, Bagryanskaya IY (2021) Synthesis and study of Re(I) tricarbonyl complexes based on octachloro-1,10-phenanthroline: towards deep red-to-NIR emitters. Polyhedron 209:115484–115499
30. Zhong F, Yuan X, Zhao J, Wang Q (2016) Visible light-harvesting tricarbonyl Re(I) complex: synthesis and application in intracellular photodynamic effect and luminescence imaging. Sci China Chem 59:70–77
31. Lo KK-W, Tsang KH-K, Zhu N (2006) Luminescent tricarbonylrhenium(I) polypyridine estradiol conjugates: synthesis, crystal structure, and photophysical, electrochemical, and protein-binding properties. Organometallics 25:3220–3227
32. Leonidova A, Pierroz V, Rubbiani R, Heier J, Ferrari S, Gasser G (2014) Towards cancer cell-specific phototoxic organometallic rhenium(I) complexes. Dalt Trans 43:4287–4294
33. Leonidova A, Pierroz V, Rubbiani R, Lan Y, Schmitz AG, Kaech A, Sigel RKO, Ferrari S, Gasser G (2014) Photo-induced uncaging of a specific Re(I) organometallic complex in living cells. Chem Sci 5:4044–4056
34. Striplin DR, Crosby GA (2001) Photophysical investigations of rhenium(I)$Cl(CO)_3$(phenanthroline) complexes. Coord Chem Rev 211:163–175
35. Ramos LD, de Macedo LH, Gobo NRS, de Oliveira KT, Cerchiaro G, Morelli Frin KP (2020) Understanding the photophysical properties of rhenium(I) compounds coordinated to 4,7-diamine-1,10-phenanthroline: synthetic, luminescence and biological studies. Dalt Trans 49:16154–16165
36. Manicum A-L, Alexander O, Schutte-Smith M, Visser HG (2020) Synthesis, characterization and substitution reactions of fac-[Re(O, O′-bid)$(CO)_3$(P)] complexes, using the "2+1" mixed ligand model. J Mol Str 1209:127953–127964
37. Manicum A-LE, Schutte-Smith M, Alexander OT, Twigge L, Roodt A, Visser HG (2019) First kinetic data of the CO substitution in fac-[Re(L, L′-Bid)$(CO)_3$(X)] complexes (L, L′-Bid = acacetylacetonate or tropolonate) by tertiary phosphines PTA and P_Ph3: Synthesis and crystal structures of water-soluble rhenium(I) tri- and dicarbonyl complexes with 1,3,5-triaza-7-phosphaadamantane (PTA). Inorg Chem Comm 101:93–98
38. Manicum A-LE, Schutte-Smith M, Visser HG (2018) The synthesis and structural comparison of fac-$[Re(CO)_3]^+$ containing complexes with altered β-diketone and phosphine ligands. Polyhedron 145:80–87
39. Manicum A, Schutte-Smith M, Kemp G, Visser HG (2015) Illustration of the electronic influence of coordinated β-diketone type ligands: a kinetic and structural study. Polyhedron 85:190–195
40. Gantsho VL, Dotou M, Jakubaszek M, Goud B, Gasser G, Visser HG, Schutte-Smith M (2020) Synthesis, characterization, kinetic investigation and biological evaluation of Re(I) di- and tricarbonyl complexes with tertiary phosphine ligands. Dalt Trans 49:35–46
41. Priyatharsini M, Mishra I, Shankar B, Srinivasan N, Krishnakumar RV, Sathiyendiran M (2021) fac-$Re(CO)_3$ core-based complex featuring benzimidazole as pendant motif from hydroxyquinoline and pyridylbenzimidazole. J Org Chem 953:122052–122062
42. Manicum A-LE, Schutte-Smith M, Malan FP, Visser HG (2022) Steric and electronic influence of Re(I) tricarbonyl complexes with various coordinated β-diketones. J Mol Str 1264:133278–133290
43. Manicum A-L, Schutte-Smith M, Visser HG, Pretorius C, Roodt A (2016) Crystal structure of tetraethylammonium fac-tricarbonyl(hexafluoroacetylacetonato-κ2O, O′)-(nitrato-κO)rhenium(I), C16H21O8N2F6Re. Zeits. für Krist. New Cryst. Str. 231:263–266
44. Lo KK-W, Louie M-W, Sze K-S, Lau JS-Y (2008) Rhenium(I) polypyridine biotin isothiocyanate complexes as the first luminescent biotinylation reagents: synthesis, photophysical properties, biological labeling, cytotoxicity, and imaging studies. Inorg Chem 47:602–611
45. Leonidova A, Gasser G (2014) Underestimated potential of organometallic rhenium complexes as anticancer agents. ACS Chem Biol 9:2180–2193
46. Mansour AM (2021) Tricarbonyl triazolato Re(I) compounds of pyridylbenzimidazole ligands: spectroscopic and antimicrobial activity evaluation. RSC Adv 11:22715–22722
47. Schindler K, Zobi F (2022) Anticancer and antibiotic rhenium tri- and dicarbonyl complexes: current research and future perspectives. Molecules 27:539–564
48. Mehler AH (1956) Formation of picolinic and quinolinic acids following enzymatic oxidation of 3-hydroxyanthranilic acid. J Biol Chem 218:241–254
49. Dazzi C, Candiano G, Massazza S, Ponzetto A, Varesio L (2001) New high-performance liquid chromatographic method for the detection of picolinic acid in biological fluids. J. Chrom. B Biol. Sci. App. 751:61–68
50. Rebello T, Lönnerdal B, Hurley LS (1982) Picolinic acid in milk, pancreatic juice, and intestine: inadequate for role in zinc absorption. Am J Clin Nutr 35:1–5

51. Peters JC (1991) Tryptophan nutrition and metabolism: an overview. Adv Exp Med & Biol 294:345–358
52. Fernandez-Pol JA, Johnson GS (1977) Selective toxicity induced by picolinic acid in simian virus 40-transformed cells in tissue culture. Can Res 37:4276–4279
53. Fernandez-Pol JA, Klos DJ, Hamilton PD (2001) Antiviral, cytotoxic and apoptotic activities of picolinic acid on human immunodeficiency virus-1 and human herpes simplex virus-2 infected cells. Anticancer Res 21:3773–3776
54. Alberto RA, Schibli R, Schubiger PA, Abram U, Kaden T (1996) Reactions with the technetium and rhenium carbonyl complexes (NEt4)2[MX3(CO)3]. Synthesis and structure of [Tc(CNBut)3(CO)3](NO3) and (NEt4)[Tc2(μ-SCH2CH2OH)3(CO)6]. Polyhedron 15:1079–1089
55. Alberto, R.; Egli, A.; Abram, U.; Hegetschweiler, K.; Gramlich, V.; Schubiger, P. A., Synthesis and reactivity of $[NEt_4]_2[ReBr_3(CO)_3]$. Formation and structural characterization of the clusters $[NEt_4][Re_3(\mu_3\text{-}OH)(\mu\text{-}OH)_3(CO)_9]$ and $[NEt_4][Re_2(\mu\text{-}OH)_3(CO)_6]$ by alkaline titration. *J. Chem. Soc., Dalt. Trans.* **1994**, 2815–2820.
56. Schibli R, La Bella R, Alberto R, Garcia-Garayoa E, Ortner K, Abram U, Schubiger PA (2000) Influence of the denticity of ligand systems on the in vitro and in vivo behavior of 99mTc(I)−tricarbonyl complexes: a hint for the future functionalization of biomolecules. Bio Chem 11:345–351
57. Rigaku O (2018) CrysAlis PRO Soft. Syst, Rigaku Corporation, Oxford
58. Sheldrick G (2015) SHELXT—Integrated space-group and crystal-structure determination. Acta Cryst Sect A 71:3–8
59. Mundwiler, S.; Kündig, M.; Ortner, K.; Alberto, R., A new [2 + 1] mixed ligand concept based on $[99(m)Tc(OH_2)_3(CO)_3]^+$: a basic study. *Dalt. Trans.* **2004**, 1320–1328.
60. Li D, Zhong G-Q (2014) Synthesis, crystal structure, and thermal decomposition of the cobalt(II) complex with 2-picolinic acid. Sci W J 2014:641608–641615
61. Manicum A-L, Alexander O, Schutte-Smith M, Visser HG, Roodt A (2017) Crystal structure of fac-(acetylacetonato-κ2O, O′)tricar bonyl(benzyldiphenylphosphine-κP)rhenium(I), C27H24O5PRe. Zeits. für Krist. New Cryst. Str. 232:957–959
62. Aleksanyan DV, Churusova SG, Rybalkina EY, Artyushin OI, Peregudov AS, Nelyubina YV, Klemenkova ZS, Bykhovskaya OV, Kozlov VA (2019) Tricarbonylrhenium(I) complexes with heterodentate ligands based on functionalized amides: synthesis, structural features, and cytotoxic activity. J Org Chem 892:66–74
63. Sovari SN, Vojnovic S, Bogojevic SS, Crochet A, Pavic A, Nikodinovic-Runic J, Zobi F (2020) Design, synthesis and in vivo evaluation of 3-arylcoumarin derivatives of rhenium(I) tricarbonyl complexes as potent antibacterial agents against methicillin-resistant *Staphylococcus aureus* (MRSA). Eur J Med Chem 205:112533
64. Hayes TR, Lyon PA, Barnes CL, Trabue S, Benny PD (2015) Influence of functionalized pyridine ligands on the radio/chemical behavior of $[MI(CO)_3]^+$ (M = Re and 99mTc) 2 + 1 complexes. Inorg Chem 54:1528–1534
65. Brink A, Visser HG, Roodt A (2013) Activation of Rhenium(I) toward substitution in fac-[Re(N, O′-Bid)$(CO_)3(HOC_H3)$] by Schiff-Base bidentate ligands (N, O′-Bid). Inorg Chem 52:8950–8961
66. Czerwieniec, R.; Kapturkiewicz, A.; Anulewicz-Ostrowska, R.; Nowacki, J., $ReI(CO)_3^+$ complexes with N∩O− bidentate ligands. *J. Chem. Soc., Dalt. Trans.* **2002**, 3434–3441.
67. Faller JW, Mason G, Parr J (2001) The synthesis of new complexes of rhenium(I) with heterotridentate [P, N, O] ligands. J Org Chem 626:181–185
68. Roodt A, Visser HG, Brink A (2011) Structure/reactivity relationships and mechanism from X-ray data and spectroscopic kinetic analysis. Cryst Rev 17:241–280
69. Booysen IN, Ebonumoliseh I, Akerman MP, Xulu B (2015) A rhenium(I) compound bearing a dimerized chromone NO bidentate chelator. Inorg Chem Comm 62:8–10
70. Schutte-Smith M, Visser HG (2015) The versatility of pyridine-2,5-dicarboxylic acid in the synthesis of fac-$M(CO)_3$ complexes (M=Re, 99mTc): reactivity towards substitution reactions and derivatization after coordination to a metal. Polyhedron 89:122–128
71. Triantis C, Shegani A, Kiritsis C, Ischyropoulou M, Roupa I, Psycharis V, Raptopoulou C, Kyprianidou P, Pelecanou M, Pirmettis I, Papadopoulos MS (2018) Dicarbonyl cis-$[M(CO)_2(N, O)(C)(P)]$ (M = Re, (99m)Tc) Complexes with a New [2 + 1 + 1] Donor Atom Combination. Inorg Chem 57:8354–8363